A MICRO - MACRO (DEM-FEM) MODEL OF THE BEHAVIOUR OF GRANULAR SOLIDS

Michał Nitka, Bilbie Bilbie, Gaël Combe, Cristian Dascalu, Jacques Desrues

Grenoble Université, Laboratory 3S-R, BP 53-38041 Grenoble cedex 9 France

ABSTRACT: *We study the macroscopic behavior of granular materials, considered as a consequence of the interactions of individual grains at the micro scale. For this, a computational homogenization approach is considered. At the small-scale level, we consider a granular structure modeled by Discrete Element Method (DEM). Grain interactions are modeled by normal and tangential contact laws with friction (Coulumb's criterion). At the macroscopic level, a numerical solution is constructed by the Finite Element Method (FEM). The upscaling technique consists in using the response of the DEM model at each Gauss point of the FEM discretisation to derive numerically the constitutive response. In this process, a tangent operator is generated together with the stress increment corresponding to the strain increment in the Gauss point. In order to get more insight on the consistency of the resulting constitutive response, we compute the determinant of the acoustic tensor associated with the tangent operator. This quantity is known to be an indicator of a possible loss of uniqueness locally, at the macro scale, by strain localization in shear bands. The results of different numerical tests are presented. Periodic boundary conditions have been compared with the ordinary wall conditions for the Representative Elementary Volume.*

1 INTRODUCTION

The presented study considers a two-scale numerical scheme for the description of the behavior of granular materials. At the small-scale level, we consider that the granular structure consists of 2D round rigid grains, modeled by the discrete element method (DEM). At the macroscopic level, we consider a numerical solution obtained with the Finite Element Method (FEM).

The link between scales is that of the computational homogenization, in which average REV stress response of the granular microstructure is obtained in each macroscopic Gauss point of the FEM mesh as the result of the macroscopic deformation history imposed to the REV. We also compute the tangent stiffness matrix, at the Gauss point, and the acoustic tensor, which is an indicator of possible unstable behaviors. The influence of different parameters on the stability of the macroscopic response is presented through the results of numerical tests.

2 MACRO LINK

2.1 Macroscopic constitutive law

For a given history of the deformation gradient, we compute the global stress response of the REV. The macroscopic stress results from the average formula $\sigma_{ij} = \frac{1}{S} \sum_{c=1}^{N_c} f_i^c \cdot l_j^c; \ \ i,j \in \{x,y\}$,

where S is the area of the sample, f_i^c and l_j^c are respectively the component i of the force acting in the contact c and the component j of the branch vector joining the mass centers of two grains in contact (Love 1927). Next, we convert the Cauchy stress into the Piola-Kirhoff stress (Bonnet & Wood 1997). The Piola-Kirchoff stress is depended on the history of the *gradient of deformation* $\mathbf{F}$ (Bilbie et al. 2007), (Bilbie et al. 2008)

$$\overline{\mathbf{P}}(t) = \Gamma^t \{\overline{\mathbf{F}}(\tau), \tau \in [0, t]\} \tag{1}$$

For any history of $\overline{\mathbf{F}}$, we assume that $\overline{\mathbf{P}}$ admits a right time derivative $\dot{\overline{\mathbf{P}}}$ with respect to t:

$$\dot{\overline{\mathbf{P}}} = lim_{\delta t \to 0} \frac{\overline{\mathbf{P}}(t + \delta t) \; - \; \overline{\mathbf{P}}(t)}{\delta t} \tag{2}$$

We also assume that, for given history of $\overline{\mathbf{F}}$ till time t, the right-sided derivative $\dot{\overline{\mathbf{P}}}$ depends only on the right time derivative $\dot{\overline{\mathbf{F}}}$, that is :

$$\dot{\overline{\mathbf{P}}} = \Theta(\dot{\overline{\mathbf{F}}}) \tag{3}$$

where the function Θ is generally non-linear with respect to its argument $\dot{\overline{\mathbf{F}}}$.

In what follows, we limit our study to the case when the history of $\overline{\mathbf{F}}$ is given by $\overline{\mathbf{F}} = \mathbf{I} + \alpha \mathbf{G^0}$ with $\mathbf{G^0}$ being a fixed tensor and α being time-like loading parameter which runs monotonously from 0 to 1. In this case we get: $\dot{\overline{\mathbf{P}}} = \Xi(\alpha)$ and by differentiating with respect to α, we get that $\dot{\overline{\mathbf{F}}} = \mathbf{G^0}$ along the path. According to the definition of the function Θ we can write the approximate formula (Bilbie et al. 2007), (Bilbie et al. 2008):

$$\Theta(\mathbf{G^0}) \approx \frac{\Xi(\alpha + \Delta\alpha) \; - \; \Xi(\alpha)}{\Delta\alpha} \tag{4}$$

2.2 *Macroscopic loss of stability - Acoustic tensor*

The loss of uniqueness for the rate-type boundary value problems is analysed through the Rice approach (Rice 1976). Following this analysis we look for the rate of deformation gradient $\dot{\overline{\mathbf{F}}}$ which is discontinuous along the boundary of a localization band. It is known that such a discontinuity can be written as (Rice 1976):

$$\dot{\overline{F_{kL}^1}} = \dot{\overline{F_{kL}^0}} + q_k N_l \tag{5}$$

where $\mathbf{N}$ is the normal ($||\mathbf{N}|| = \mathbf{1}$) to the interface, $\dot{\overline{\mathbf{F^1}}}$ is taken on the same side as $\mathbf{N}$ and $\dot{\overline{\mathbf{F^0}}}$ on the opposite side. The stress vector has to be continuous across the interface :

$$\left(\dot{\overline{P_{iJ}^1}} \; - \; \dot{\overline{P_{iJ}^0}} \right) N_J \; = \; 0 \tag{6}$$

As $\dot{\overline{P_{iJ}^1}}$ and $\dot{\overline{P_{iJ}^0}}$ are linked to $\dot{\overline{F_{iJ}^1}}$ and, respectively, $\dot{\overline{F_{iJ}^1}}$, by Eq. (3), the unknowns $\mathbf{q}$ and $\mathbf{N}$ have to satisfy the equation

$$\left(\Theta_{iJ} \left(\dot{\overline{\mathbf{F^0}}} + \mathbf{q} \otimes \mathbf{N} \right) - \Theta_{iJ} \left(\dot{\overline{\mathbf{F^0}}} \right) \right) N_J = 0 \tag{7}$$

for given $\dot{\overline{\mathbf{F^0}}}$.

In the considered macroscopic quasistatic deformation process, the question of loss of ellipticity therefore reduces to the determination of the value α for which Eq. (7) has a non-trivial solution

$(\mathbf{q}, \mathbf{N})$, $\mathbf{q} \neq \mathbf{0}$.

In our case we restrict the search of non-trivial solutions to the case in which the tensor $\dot{\overline{\mathbf{F}^1}}$ is closed to $\overline{\mathbf{F}^0}$. This leads to a continuous bifurcation mode in the sense of Rice (Rice 1976).

So, assuming that Θ is differentiable at $\dot{\overline{\mathbf{F}^0}}$, Eq. (7) yields, after linearization:

$$B_{iJkL}\left(\dot{\overline{\mathbf{F}^0}}\right) q_k N_L N_J = 0 \tag{8}$$

where $B_{iJkL}\left(\dot{\overline{\mathbf{F}^0}}\right) = \frac{\partial \Theta_{iJ}}{\partial \dot{F}_{kl}}\big|_{\dot{\mathbf{F}}=\dot{\overline{\mathbf{F}^0}}}$ It is clear that a non-trivial solution exists only if the so-called *acoustic tensor* $\mathbf{Q}$, defined by $Q_{ik} = B_{iJkL}N_L N_J$, is singular, that is only if:

$$det\mathbf{Q} = \mathbf{0} \tag{9}$$

For this particular process considered here and given by $\overline{\mathbf{F}} = \mathbf{I} + \alpha\mathbf{G^0}$, we have seen that $\dot{\overline{\mathbf{F}}}$ is constant and equal to $\mathbf{G^0}$ and the function $\Theta(\mathbf{G^0})$ can be approximated by Eq.(4).

As to the derivation of Θ, it can be numerically approximated by finite differences:

$$B_{iJkL} = \frac{\Theta_{iJ}(\mathbf{G}^0 + \varepsilon\Delta^{kL}) - \theta_{iJ}(\mathbf{G^0})}{\varepsilon} \tag{10}$$

where Δ^{kL} is a second-order tensor such that all its components are equal to 0 except the *kL* one which is equal to 1. In Fig. 1) we have represented the stress at the point $\delta f \Delta \alpha$ (in the same linear direction as point n) and stresses in points with perturbations $\varepsilon\Delta^{kL}$. We also computed the tangent matrix (Bilbie et al. 2007), (Bilbie et al. 2008) as :

$$B_{iJkL} = \frac{P_{iJ}(\alpha^{n+1} + \delta f \Delta \alpha + \varepsilon\Delta^{kL}) - P_{iJ}(\alpha^{n+1} + \delta f \Delta \alpha)}{\delta f \, \varepsilon\Delta^{kL}} \tag{11}$$

where $\delta f \Delta \alpha$ is a small variation step in the main direction, $\varepsilon\Delta^{kL}$ is a small perturbation in the direction *kL*.
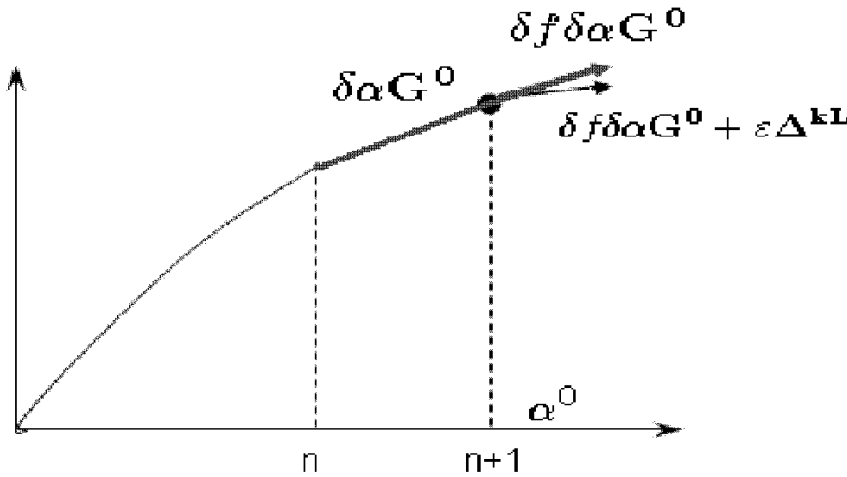
Fig. 1. Schematic representation of the computation of the tangent matrix

3   MICRO-SCALE MODELING: DEM

The system consist of a set of N polydisperse discs, with the random radii homogeneously distributed between R_{min} and $R_{max} = 2.5R_{min}$. This system is simulated using a discrete element method - molecular dynamics with a third-order predictor-corrector scheme (Allen & Tildesley 1994). All grains interact via a linear elastic law and Coulomb friction when they are in contact (Cundal & Strack 1979). The normal contact force f_n is related to the normal apparent interpenetration δ of the contact as $f_n = k_n\delta$, where k_n is a normal stiffness coefficient ($\delta > 0$ if a contact is present, $\delta = 0$ if there is no contact). The tangential component f_t of the contact force is proportional to the tangential elastic relative displacement, with a tangential stiffness coefficient k_t. The Coulomb condition $|f_t| \leq \mu f_n$ requires an incremental evaluation of f_t in each time step, which leads to some amount of slip each time one of the equalities $f_t = \pm\mu f_n$ is imposed. A normal viscous component opposing the relative normal motion of any pair of grains in contact is also added to the elastic force f_n to obtain a critical damping of the dynamics. We consider two different boundary conditions: *Periodic Limit Condition* (PLC) and *rigid wall* (WLC), cf. Fig.2
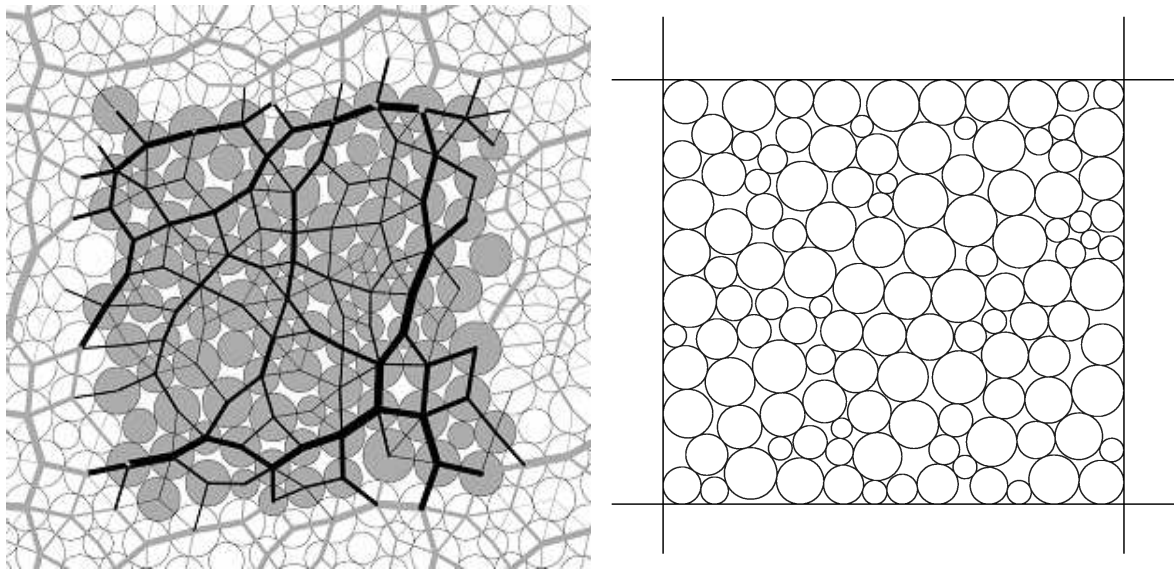
Fig. 2. Shape of the PLC sample with normal contact forces (left) and cell of the sample with rigid walls (right)

The idea of PLC is that every grain is not only in contact with neighbours it the simulated cell (primary box), but also with some grains in 'image cell' which are replicated to infinity by rigid translations in 2D Cartesian directions. This replicas contain the same sets of grains as the primary cell (Ellero 2004). Finally, if one grain is moving out of primary cell, it appears on the opposide side of cell - with the same velocity and the same momentum.

Both *PLC* and *WLC* conditions were implemented. In every step we applied an increment of strain and, after DEM computations, we recover the stresses.

We have considered different sizes of the samples (from 400 grains to 9801) and different velocities of the applied strains and we analyzed their influence on the behavior of the sample and the stress response.

4 RESULTS

The normal stiffnes of contact in the DEM is calculated for the 2D, where stiffness parameter (Combe & Roux) $\kappa = \frac{k_n}{\sigma_0}$, where k_n is a stiffness and $\sigma 0$ is an isotropic stress applied to the grain assembly. The value of κ is taken 1000, that corresponds to quite rigid bodies. The value of the tangential stiffness is equal to the normal stiffness $k_t = k_n$. Friction coefficient is taken as $\mu = 0.5$. We have considered different boundary conditions, different sizes of the samples (number of grains), and different velocities of the applied strains.

The first example is a *biaxial* test without volume changes. The final strain matrix is $\varepsilon = \begin{bmatrix} 0.2 & 0 \\ 0 & -0.2 \end{bmatrix}$, where negative sign is for compression. We have performed 10 tests for each size of the sample and we have calculated mean stress and its standard deviations. We have done it for both types of boundary conditions: *PLC* and *WLC*. The stress-strain response resulting for different size of the sample are presented in Fig. 3 and Fig. 4 for *PLC* and *WLC*, respectively. The y-axis is a $\frac{q}{p}$, where $q = \frac{\sigma_{yy} - \sigma_{xx}}{2}$ and p is a mean value of stress $p = \frac{\sigma_{yy} + \sigma_{xx}}{2}$. In the diagram Fig.3 and 4 one can see standard deviations of the sample for the $\frac{q}{p}$.
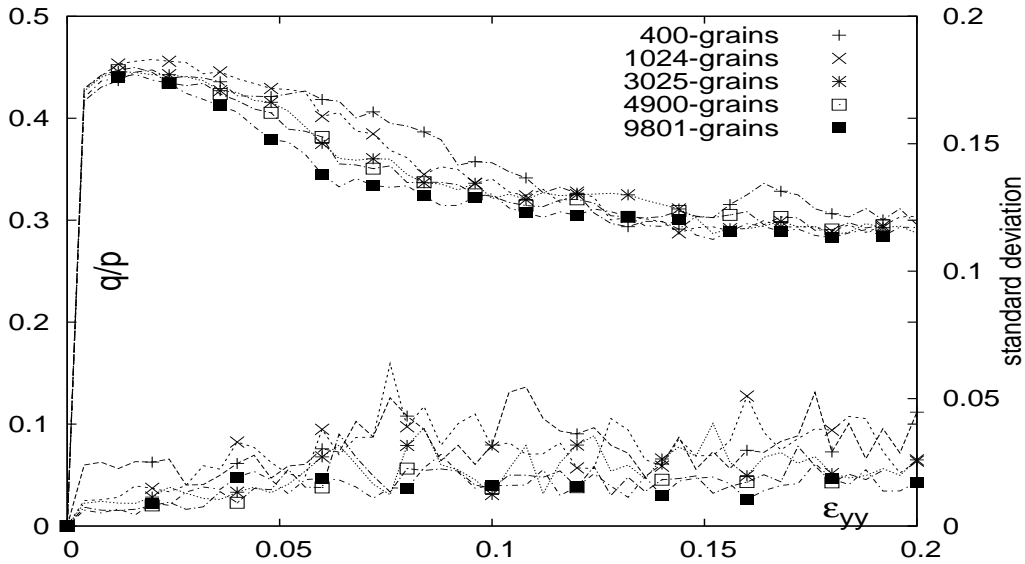
Fig. 3. Mean stress and standard deviation of PLC samples

We can observe that, for PLC and WLC, mean stress is increasing when the number of grains is decreasing, but the difference is small. On the other hand the standard deviation is decreasing with increase of the sample size and over 3025 grains it is established (Fig. 3 and 4), but for PLC samples there is less noise.

A second series of tests was made to check the influence of the velocity of the applied strain. It was done by changing the so-called *Inertial number* $I = \dot{\varepsilon} \sqrt{\frac{<m>}{\sigma_0}}$ (Roux & Chevoir 2005), where $\dot{\varepsilon}$ is a velocity of strain, $< m >$ is the mean mass of grains and σ_0 is the stress in the isotropic state. In figure 5 different I (beetwen $5, 6 \cdot 10^{-3}$ and $2, 8 \cdot 10^{-5}$) are presented. It was done for a sample cell with 3025 grains, for the final strain matrix $\varepsilon = \begin{bmatrix} 0.2 & 0 \\ 0 & -0.2 \end{bmatrix}$ (test with no volume changes). One can observe that, for the strain-stress diagram, the influence of I is rather small. This is due to the fact that in the code there is strong equilibrium condition.

Next, we performed tests for checking the stability in the macro level (biaxial test with and without volume changes, uniaxial and shearing). They were done for samples with 400, 1024,
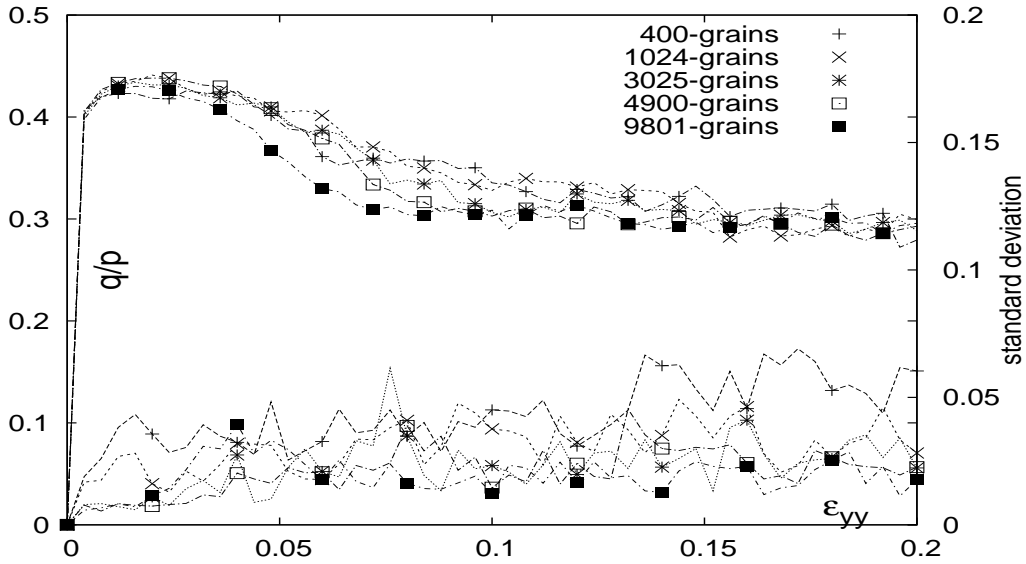
Fig. 4. Mean stress and standard deviation of WALL samples
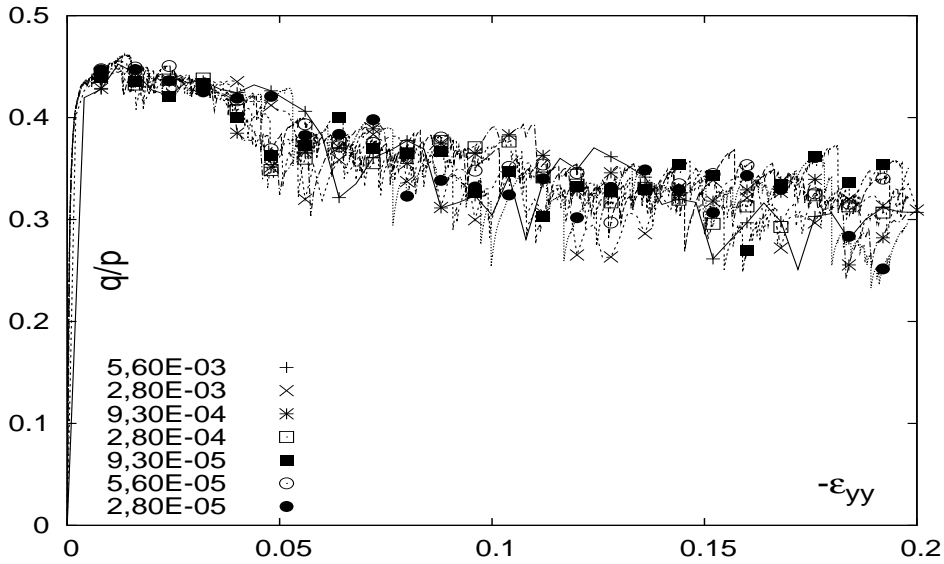
Fig. 5. Different inertial number I for sample with 3025 grains

3025 and 4900 grains.

The influence of the sample size for shearing test for stress $P - K_{12}$ is presented in Fig. 6 (to be more clear, the diagrams were moved up on y-axis). Stars represent instability zones, that correspond to the $det\mathbf{Q} < \mathbf{0}$, where Q is the acoustic tensor. This test was made for $\delta f = 0.1$ and perturbation $\varepsilon \Delta^{kL} = 2 \cdot 10^{-6}$.

One can observe that if the size of sample is increasing we obtain more important stability zones. All tests were done with similar *Inertial number* $I = \dot{\varepsilon}\sqrt{\frac{<m>}{\sigma_0}}$. **I** was set between $1.2 \cdot 10^{-3}$ to $2.1 \cdot 10^{-3}$ for iterations, and $1.2 \cdot 10^{-4}$ to $2.1 \cdot 10^{-}4$ for the small variation step $\delta f \delta \alpha$.

We have also done tests to check the influence of the size of the small variation step $\delta f \delta \alpha$ and the small perturbations $\varepsilon \Delta^{kL}$. We have done it for shearing test for sample with 3025 grains. First, the perturbation was taken as $2 \cdot 10^{-6}$. Values for the small variation step δf were be-
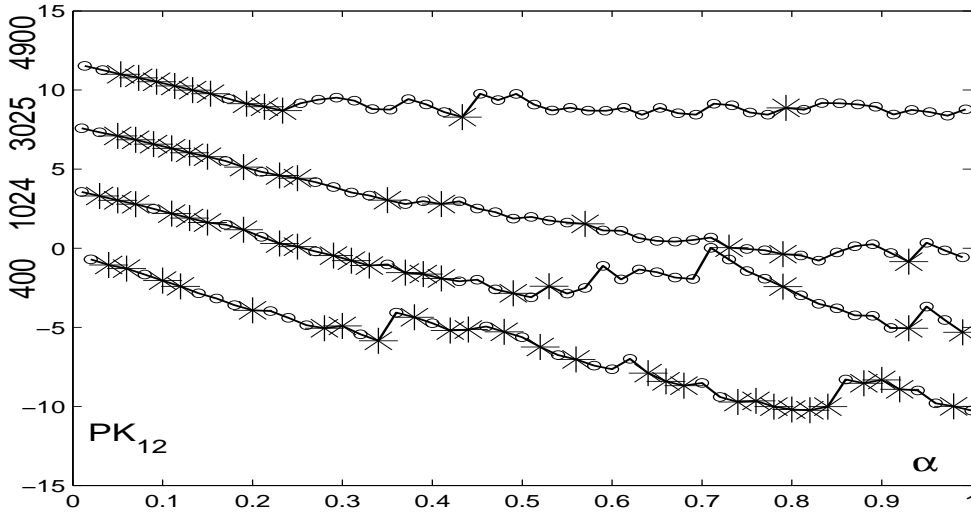
Fig. 6. Influence of the size of sample on macroscopic stability

tween 0.05 to 1 (Fig. 7). Next, the small variation step was constant and equal to 0.01, but the perturbation step was between $2 \cdot 10^{-6}$ to $2 \cdot 10^{-3}$ (Fig. 8).
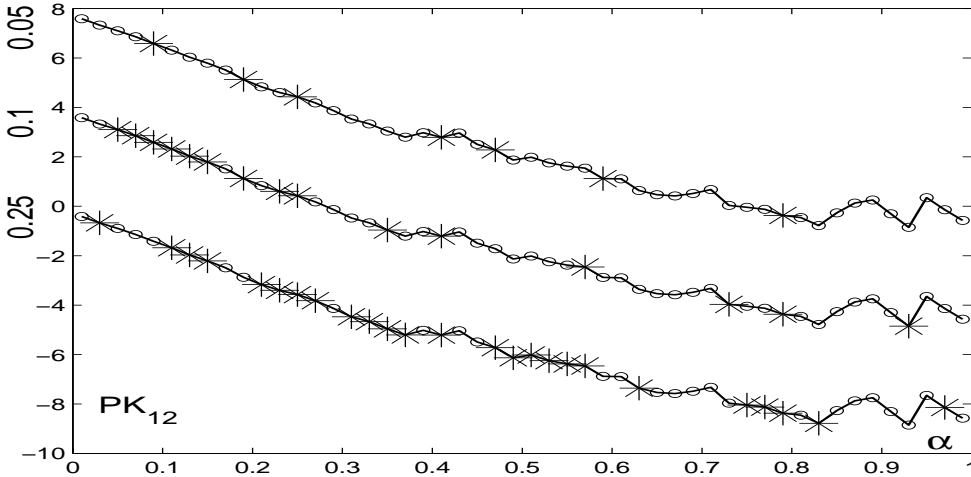
Fig. 7. Influence of the variation step on macroscopic stability

In this case we have obtained larger stability zones for smaller values of small variation step $\delta f \delta \alpha$ and for smaller values of perturbation value. But, it is important to take the value of $\delta f \delta \alpha$ carefully to be still in elasto-plasticy behaviour (not only elasticity).

One important point is the identification of the microscopic origins for the macro instabilities. To do this we are using the so-called *fluctuations of displacement of grains* $\boldsymbol{\delta}_i^{mn} = (\boldsymbol{r}_i^n - \boldsymbol{r}_i^m) - \Delta \varepsilon \boldsymbol{r}_i^m$, where $\boldsymbol{r}_i^m, \boldsymbol{r}_i^n$ are the position of grain i in step m and n, respectively and $\Delta \varepsilon$ is a tensor of the increment of the strain from step m to n. Next we compute the mean value of fluctuation for all grains in the cell for one iteration ($\Delta \varepsilon_{xy}$ isn constant): $\langle \delta^{mn} \rangle = \frac{1}{N} \sum_{i=1}^{N} \| (\delta_i^{mn}) \|^2$ where N is the number of grains.
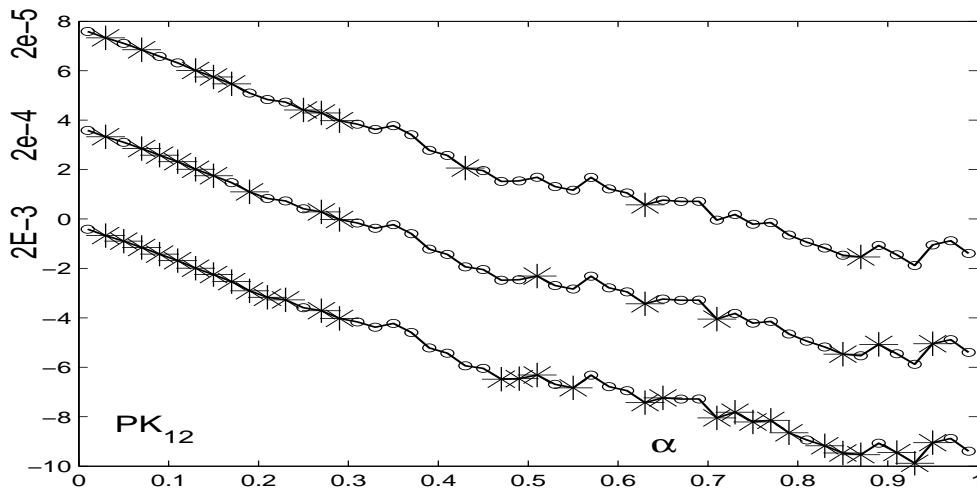
Fig. 8. Influence of the perturbation value on macroscopic stability
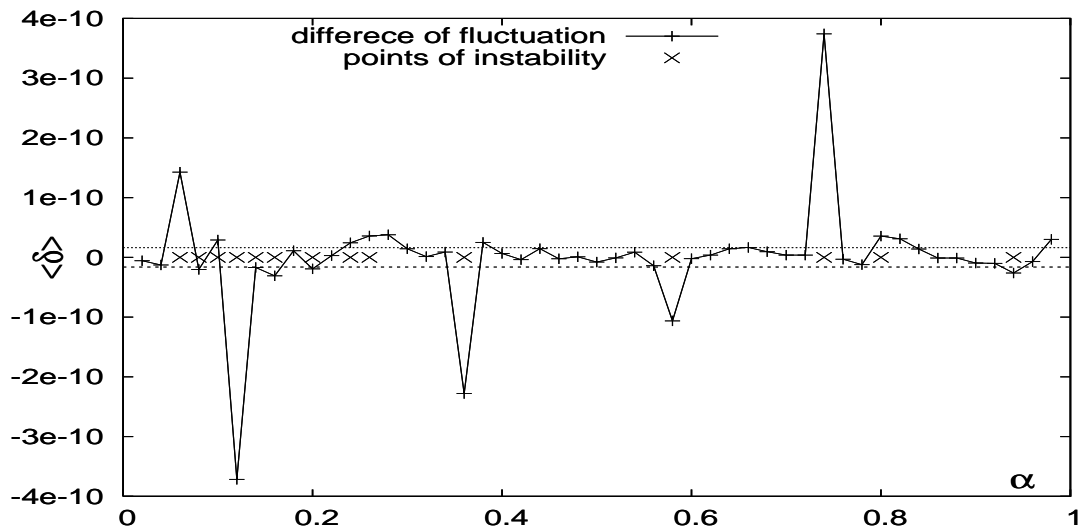
Fig. 9. Difference of the fluctuation of the grains (crosses correspond with the instability points)

In figure 9 we can observe changing of the fluctuation of the grains in the sample with 3025 particles in shearing. The diagram prezents the differance beetwen the fluctuation of grains in small variation step and mean fluctuation of all four perturbations. We can observe that, if the difference is big, we get points of instability.

In figure 10 are presented maps of the fluctuations in two different points. On the top there is map for a stability point and on the bottom for a point of instability. One can observe that for the unstable case in some part of the sample we have bigger fluctuations of grains and they are more chaotically distributed . We have not noticed that kind of behaviour in stability points.

5 CONCLUSIONS

A two-scale numerical approach for granular materials has been proposed, combining DEM modelling of the granular microstructure with the FEM modeling of the overall response. We focused on the consistency of the discrete-to-continuous approach, through the identification of
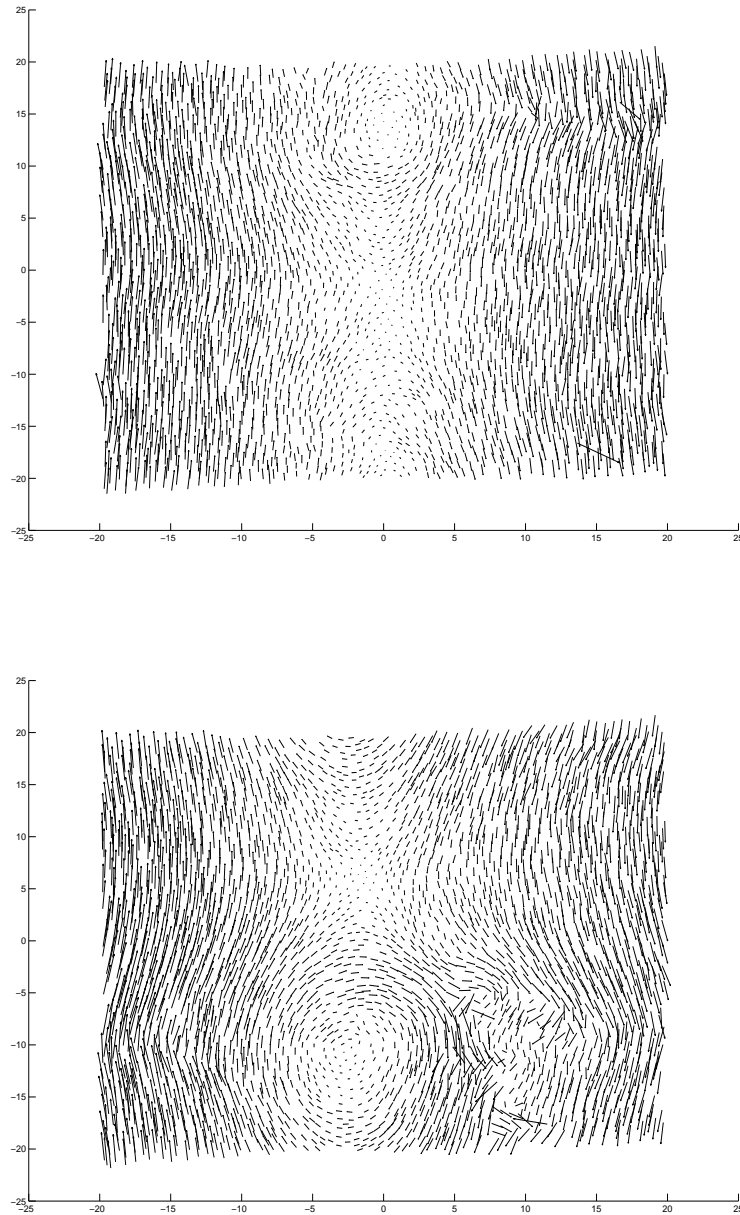
Fig. 10. Maps of displacement for variation step for stability (top) and instability (bottom) points

the numerically-induced macroscopic instabilities.

We can observe that boundary conditions have influences on mean stress and standard deviation, but this influence is relatively small. For the mean stresses for PLC, the sample size does not play an important role, but for stability zones it has huge influence. In order to not induce "numerical instabilities", it is very important to make the correct choice for the size of the sample (not too small). It is also very important to choose the correct small variation step δf and small perturbation $\varepsilon \Delta^{kL}$.

At the small-scale level, we observed a behaviour dependent on this coefficients, allowing us to identify the origin of instabilities in the macroscopic response. In the instability regime, some grains loose their contact during small variation steps and perturbations. Such microscopic be-

haviour may be a true physical behaviour, linked to instability and shear banding. As such, it should not be rejected in general. But the occurrence of such events far from the failure regime of the sample, if not limited to a few points but spread over the sample in a significant number of points, may indicate non-relevant numerical behaviour. This is a challenge to deal with, maybe by exploring more changes in the numerical parameters. After a convenient resolution of this problem, it is possible to perform two-scale FEM-DEM computations, for more complicated samples.

REFERENCES

Allen, M. P. & Tildesley, D. J. (1994). Computer simulation of liqiuds. *Oxford Science Publications*.

Bilbie, G., Dascalu, C., Chambon, R., & Caillerie., D. (2007). Micro-fracture instabilities in granular solids. *in Bifurcations, Instabilities, Degradation in Geomechanics, Exadaktylos G. and Vardoulakis I. eds., pp. 231-242*.

Bilbie, G., Dascalu, C., Chambon, R., & Caillerie., D. (2008, oct). Micro-fracture instabilities in granular solids. *Acta Geotechnica, vol.3, pages 25-35*.

Bonnet, J. & Wood, R. D. (1997). *Nonlinear continuum mechanics for finite element analysis*. Cambridge University.

Combe, G. & Roux, J.-N. Microscopic origins of quasi-static deformation in dense granular assemblies. *Powder and Grains 2001, Y. Kishoni, Ed., Balkema*, 293–296.

Cundal, P. A. & Strack, O. D. L. (1979). A discrete numerical model for granular assemblies. *Geotechnique 29*, 47–65.

Ellero, M. (2004). Smoothed Particle Dynamics Methods for the Simulation of Viscoelastic Fluids. *Berlin, PhD*.

Love, A. (1927). *A treatise on the mathematical theory of elasticity*. Cambridge University Press.

Rice, J. (1976). The localization of plastic deformation. *Koiter WT (ed) Theoretical and applied mechanics*, 207–220.

Roux, J.-N. & Chevoir, F. (2005). Discrete numerical simulations and mechanical behavior of granular materials. *Bulletin des Laboratoires des Pontes et Chaussees, 245*, 109–138.